

# Enhancing Ambient Backscatter Communication Utilizing Coherent and Non-Coherent Space-Time Codes

Wenjing Liu, *Student Member, IEEE*, Shanpu Shen, *Member, IEEE*,  
Danny H. K. Tsang, *Fellow, IEEE*, Ross Murch, *Fellow, IEEE*

**Abstract**—Ambient backscatter communication (AmBC) leverages the existing ambient radio frequency (RF) environment to implement communication with battery-free devices. The key challenge in the development of AmBC is the very weak RF signals backscattered by the AmBC Tag. To overcome this challenge, we propose the use of orthogonal space-time block codes (OSTBC) by incorporating multiple antennas at the Tag as well as at the Reader. Our approach considers both coherent and non-coherent OSTBC so that systems with and without channel state information can be considered. To allow the application of OSTBC, we develop an approximate linearized and normalized multiple-input multiple-output (MIMO) channel model for the AmBC system. This MIMO channel model is shown to be accurate for a wide range of useful operating conditions. Two coherent detectors and a non-coherent detector are also provided based on the proposed AmBC channel model. Simulation results show that enhanced bit error rate performance can be achieved, demonstrating the benefit of using multiple antennas at the Tag as well as the Reader.

**Index Terms**—Ambient backscatter communication, coherent detection, multiple-antenna Tag, multiple-antenna Reader, non-coherent detection, orthogonal space-time block codes.

## I. INTRODUCTION

**B**ACKSCATTER communication has a long history [1], [2] and an important application is Radio Frequency (RF) Identification. Typically in backscatter communication systems, a “Reader” transmits signals to a “Tag”, which harvests energy from the received signals to power its circuits and backscatter the signals to the Reader through tuning its load impedance [3]-[5]. The key advantage of backscatter communication is that the Tag does not require a battery and can be inexpensive to construct. However, there are some disadvantages that limit the use of backscatter communication. These include the need for a dedicated source of RF radiation as well as a frequency spectrum allocation to allow the system to operate.

To address the disadvantages of conventional backscatter communication, ambient backscatter communication (AmBC) systems have been proposed [6]. Compared with traditional

backscatter systems, AmBC harnesses ambient RF signals transmitted from existing wireless systems (such as DTV [6], FM [7], [8], and Wi-Fi [9]-[12]) as sources of RF radiation. This allows AmBC to operate without any dedicated RF source or extra frequency spectrum allocation and makes it a promising technology for applications such as the Internet-of-Things (IoT).

A significant challenge of AmBC is that the ambient RF waves are unknown and uncontrollable and the backscattered signals are often very weak. To solve this issue, an averaging mechanism has been proposed [6] to eliminate the influence of the ambient signals. Based on this idea, energy detection with detection thresholds and bit error rate (BER) expressions have been developed [13], [14]. Differential encoding and non-coherent energy detectors have also been designed, which do not require any channel state information (CSI) and pilot symbols [15], [16]. The non-coherent energy detector has also been generalized to MPSK [17]. Instead of averaging the ambient RF signals, FSK [18], [19] has been proposed so that the backscattered signals shift to a band that does not overlap the ambient RF signals. In [20], matched-filtering at the Tag is utilized to estimate ambient waves as well as detect backscattered signals. Coding mechanisms have also been utilized in AmBC systems, including a three states coding scheme [21] to improve throughput as well as Manchester coding [22] to reduce the decoding delay. Moreover, performance analysis in terms of resource allocation and scheduling have been proposed [23]-[26]. In [24], [25], time switching and power splitting architectures have been optimized to achieve optimal outage and throughput performance. Aspects related to ergodic capacity and outage probability have also been studied [27]-[30]. In [31], [32], the BER and capacity of a Tag selection scheme has been explored and in [33], throughput of a multitag AmBC system has been considered. AmBC has also been incorporated with RF-powered cognitive radio networks and the secondary network throughput has been significantly improved [34], [35]. In addition, the concepts of energy efficiency and hardware efficiency for AmBC have also been introduced [35], [36].

To further enhance backscattered signal detection performance, multiple antennas have been proposed at the Reader so that diversity gain can be leveraged [37]-[47]. Specifically, a dual-antenna Reader and a ratio detector have been proposed [37] to extend the transmission distance. Based on these results [37], the ratio detector has been re-investigated [38] and the

Manuscript received; This work was supported by the Hong Kong Research Grants Council under General Research Fund grant 16207620. (*Corresponding author: Shanpu Shen.*)

W. Liu, S. Shen, D. H. K. Tsang and R. Murch are with the Department of Electronic and Computer Engineering, The Hong Kong University of Science and Technology, Clear Water Bay, Kowloon, Hong Kong (e-mail: wliubj@connect.ust.hk; sshenaa@connect.ust.hk; eetsang@ust.hk; eermurch@ust.hk).

corresponding decision threshold when the Reader has more than two antennas has been found. The problem of noise uncertainty in multiple-antenna Reader AmBC systems has also been solved [39]. By using receive beamforming at a multiple-antenna receiver [40], and by a constellation-learning method [41], direct-link interference is mitigated and CSI can be avoided. Multi-antenna frequency diverse arrays have been employed to improve channel capacity [42]. In addition, a cooperative AmBC system [43], an adaptive AmBC system [44], and AmBC systems leveraging ambient orthogonal frequency division multiplexing (OFDM) modulated signals [45]-[47], all with multiple-antenna Readers, have been proposed to enhance AmBC system performance.

Using multiple antennas at the Tag can also provide diversity gain to enhance signal detection performance, however, there are only a few studies considering this. Compared with using multiple antennas at the Reader, multiple antennas at the Tag can increase the backscattered signal power and the amount of ambient RF energy that can be harvested [48]. It should be noted however that increasing antenna directivity at the Tag through using RF combining or large antennas cannot straightforwardly improve backscatter. This is because the antenna will become directive with the main beam potentially pointing away from the Reader and reducing backscatter to the Reader. Therefore, more advanced approaches must be used for multiple-antenna Tags. An AmBC system with different power allocations on two Tag antennas has been proposed [49] to increase link reliability. However, an 8-bit preamble is required to calculate the decision threshold, and CSI at the Reader (CSIR) is required. In recent studies [50], [51], a multiple-antenna Tag has been proposed where antenna selection is performed to increase the diversity gain of the AmBC system, and the information is recovered utilizing the difference in signal power statistics. However, the proposed approaches [50], [51] achieve optimal performance based on knowing the order of the channel gains at the Tag, which means that partial CSI at the Tag (CSIT) is required. Hence, pilot symbols and feedback from the Reader to Tag are required, which increases power consumption, time delay, and system complexity.

### A. Motivation and Contributions

The majority of the work reviewed [13]-[47] only uses a single antenna at the Tag. Only a few works [49]-[51] consider using multiple antennas at the Tag, but these works only use a single antenna at the Reader and therefore, receive diversity gain has not been leveraged. In addition the majority of the previous work using multiple antennas also require CSI knowledge [37], [38], [43]-[45], [49]-[51]. For example, CSIR [49] and CSIT [50], [51]. However, estimating CSI increases the complexity and power consumption of AmBC.

To the best of our knowledge there is no work using multiple antennas at both the Tag and Reader that leverage conventional multiple-input multiple output (MIMO) techniques to enhance signal detection performance in AmBC systems. Performing this would deliver power gain, transmit diversity gain, receive diversity gain and enhance signal detection in AmBC. Methods

for providing it with low complexity and without requiring CSIR or CSIT would also be desirable.

In this paper, we propose using a multiple-antenna Tag and a multiple-antenna Reader in AmBC by applying coherent and non-coherent orthogonal space-time block codes (OSTBC) to enhance the detection performance. Specifically our contributions include:

1) Using multiple antennas both at the Tag and at the Reader: We propose using multiple antennas at both the Tag and Reader to form a MIMO AmBC system, so as to jointly leverage power gain, transmit diversity gain, and receive diversity gain to enhance signal detection in AmBC. We show through both theoretical analysis and simulation results that using multiple antennas at both sides can significantly lower the BER and increase the total harvested energy. To the authors' best knowledge, this is the first work which proposes a MIMO AmBC system to enhance signal detection performance.

2) Proposing a linear MIMO channel model for the multiple antenna Tag and Reader system: In particular we derive an accurate AmBC channel model that can be applied to any MIMO AmBC communication scenario. Due to the MIMO AmBC channels nonlinear nature we develop an approximate linear MIMO AmBC channel model to simplify the detection process so that any conventional MIMO technique can be utilized. This is a key contribution in enabling MIMO AmBC.

3) Utilizing coherent and non-coherent orthogonal OSTBC: OSTBC is a well-known MIMO technique with a straightforward encoding design and low decoding complexity, which can provide full spatial diversity. However, the application of OSTBC to AmBC has been noted previously as an open problem [51]. By leveraging our linear AmBC MIMO model this can be overcome. Furthermore, noting that CSI is not always available in AmBC systems, we consider both coherent and non-coherent OSTBC. When CSI is available, we utilize coherent OSTBC to enhance the system performance with low complexity and the general performance metrics for OSTBC under AmBC system have been given. When CSI is not available, we utilize differential OSTBC and neither CSIR nor CSIT is needed, which reduces the complexity and power consumption and outperforms other work using multiple antennas on the Tag. To our best knowledge, this is the first work using multiple antennas on the Tag and on Reader without requiring any knowledge of CSI. For both cases, analysis and simulation results are provided to verify the performance of our approach.

### B. Organization and Notation

In Section II, an accurate channel model of the AmBC system with a multiple-antenna Tag and a multiple-antenna Reader is presented. In Section III, we propose the use of linearization and normalization to provide a linearized and normalized MIMO channel model for the proposed AmBC system. Using the proposed AmBC MIMO channel model we apply coherent and non-coherent OSTBC to AmBC systems and provide their corresponding detectors in Sections IV and V, respectively. Section VI provides simulation results and Section VII concludes the paper.

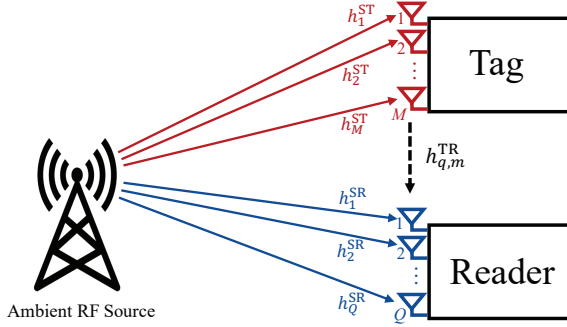


Fig. 1. System model for an AmBC system with a multiple-antenna Tag and a multiple-antenna Reader.

Bold lower and upper case letters denote vectors and matrices, respectively. A symbol not in bold font represents a scalar.  $\mathbb{E}[\cdot]$  refers to expectation.  $x^*$ ,  $\Re\{x\}$ ,  $\Im\{x\}$  and  $|x|$  refer to the conjugate, real part, imaginary part and modulus of a complex scalar  $x$ , respectively.  $\|\mathbf{x}\|$  refers to the  $l_2$ -norm of a vector  $\mathbf{x}$ .  $\mathbf{X}^T$  and  $\mathbf{X}^H$  refer to the transpose and conjugate transpose of a matrix  $\mathbf{X}$ , respectively.  $\mathcal{N}(\mu, \sigma^2)$  and  $\mathcal{CN}(\mu, \sigma^2)$  refer to the Gaussian distribution and the circularly symmetric complex Gaussian distribution with mean  $\mu$  and variance  $\sigma^2$ , respectively.  $\xrightarrow{d}$  refers to the convergence in distribution.  $Q(\cdot)$  refers to the Q function.

## II. AMBIENT BACKSCATTER COMMUNICATION SYSTEM

### A. System Model

Consider an AmBC system consisting of an ambient RF source, a passive Tag equipped with  $M$  antennas and a Reader equipped with  $Q$  antennas as shown in Fig. 1. The ambient RF signal is denoted by  $s(n)$  with symbol period  $T_a$  where  $n = 1, 2, \dots$  is the symbol index of the ambient source.  $s(n)$  is assumed random (and may come from different RF sources) and is assumed to follow a circularly symmetric complex Gaussian distribution  $\mathcal{CN}(0, P_s)$ , where  $P_s$  denotes the average power of the ambient RF signal [16]. For the  $n$ th symbol period of the ambient source, the signal received by the  $q$ th Reader antenna from the ambient RF source is expressed as

$$r_q(n) = A_{\text{SR}} h_q^{\text{SR}} s(n), \quad (1)$$

where  $A_{\text{SR}}$  and  $h_q^{\text{SR}}$  respectively denote the large- and small-scale channel fading between the ambient RF source and the  $q$ th Reader antenna, i.e.  $h_q^{\text{SR}} \sim \mathcal{CN}(0, 1)$ . The signal received by the  $m$ th Tag antenna from the ambient RF source is expressed as

$$t_m(n) = A_{\text{ST}} h_m^{\text{ST}} s(n), \quad (2)$$

where  $A_{\text{ST}}$  and  $h_m^{\text{ST}}$  denote the large- and small-scale channel fading between the ambient RF source and the  $m$ th Tag antenna, i.e.  $h_m^{\text{ST}} \sim \mathcal{CN}(0, 1)$ . The signal backscattered by the  $m$ th Tag antenna can be expressed as

$$d_m(n) = \alpha x_m t_m(n), \quad (3)$$

where  $\alpha$  denotes the hardware implementation loss of the Tag and  $x_m$  refers to the symbol transmitted by the  $m$ th

Tag antenna using backscattering [49]-[51]. The total signal received by the  $q$ th Reader antenna can be expressed as

$$\begin{aligned} z_q(n) &= r_q(n) + \sum_{m=1}^M A_{\text{TR}} h_{q,m}^{\text{TR}} d_m(n) + w_q(n) \\ &= \left( A_{\text{SR}} h_q^{\text{SR}} + \alpha A_{\text{TR}} A_{\text{ST}} \sum_{m=1}^M h_{q,m}^{\text{TR}} h_m^{\text{ST}} x_m \right) s(n) + w_q(n), \end{aligned} \quad (4)$$

where  $A_{\text{TR}}$  and  $h_{q,m}^{\text{TR}}$  denote the large- and small-scale channel fading between the  $m$ th Tag antenna and the  $q$ th Reader antenna, and  $w_q(n)$  is the additive white Gaussian noise (AWGN) at the  $q$ th Reader antenna, i.e.  $h_{q,m}^{\text{TR}} \sim \mathcal{CN}(0, 1)$ ,  $w_q(n) \sim \mathcal{CN}(0, 1)$ .

We assume  $h_q^{\text{SR}}$ ,  $h_{q,m}^{\text{TR}}$ , and  $h_m^{\text{ST}} \forall m$  and  $q$  are independent and identically distributed (i.i.d.), quasi-static, and frequency flat. We also assume  $A_{\text{SR}} \approx A_{\text{ST}}$  since the Tag and the Reader are close to each other. Therefore, we can normalize (4) by  $A_{\text{SR}}$  to equivalently rewrite (4) as

$$\bar{z}_q(n) = (h_q^{\text{SR}} + \mathbf{h}_q^{\text{TR}} \mathbf{G} \mathbf{x}) s(n) + \bar{w}_q(n), \quad (5)$$

where we define  $\bar{z}_q(n) = z_q(n)/A_{\text{SR}}$ ,  $\bar{w}_q(n) = w_q(n)/A_{\text{SR}}$ ,  $\mathbf{x} = [x_1, x_2, \dots, x_M]^T$ ,  $\mathbf{h}_q^{\text{TR}} = [h_{q,1}^{\text{TR}}, h_{q,2}^{\text{TR}}, \dots, h_{q,M}^{\text{TR}}]$ , and  $\mathbf{G} = \alpha A_{\text{TR}} \text{diag}(h_1^{\text{ST}}, h_2^{\text{ST}}, \dots, h_M^{\text{ST}})$ . We assume  $\bar{w}_q(n) \sim \mathcal{CN}(0, \sigma^2)$  where  $\sigma^2$  denotes the normalized noise power and  $\mathbf{x}$  is referred to as the Tag transmit signal. It is important to note that  $|x_m| \leq 1$  due to the passive backscattered reflection so that we have

$$\mathbb{E}[\|\mathbf{x}\|^2] \leq P_T = M, \quad (6)$$

where  $P_T$  denotes the maximum transmit power backscattered from the Tag. Different from conventional MIMO communications, where  $P_T$  is a constant, in AmBC  $P_T$  linearly increases with the number of Tag antennas  $M$ . Therefore, using multiple-antenna Tag brings extra power gain in addition to diversity and multiplexing gain in conventional MIMO.

Leveraging (5), we can define direct link signal-to-noise ratio (SNR)  $\gamma_a$  as

$$\gamma_a = \frac{P_s}{\sigma^2}, \quad (7)$$

which is the ratio of ambient RF signal power and normalized noise power at the Reader, and define a relative SNR  $\Delta\gamma$  as

$$\Delta\gamma = \frac{1}{\alpha^2 A_{\text{TR}}^2}, \quad (8)$$

which is the ratio of the signal power from the direct link and the backscatter link.

Since the ambient RF signal  $s(n)$  is unknown, it is challenging to detect the transmit signal  $\mathbf{x}$  from  $\bar{z}_q(n)$ . To overcome this challenge, we consider leveraging the statistics of  $\bar{z}_q(n)$  to detect  $\mathbf{x}$ , as  $s(n)$  is assumed as Gaussian. Because  $s(n)$  and  $\bar{w}_q(n)$  are independent circularly-symmetric complex Gaussian random variables, we can find the distribution of  $\bar{z}_q(n)$  as

$$\bar{z}_q(n) \sim \mathcal{CN}\left(0, P_s |h_q^{\text{SR}} + \mathbf{h}_q^{\text{TR}} \mathbf{G} \mathbf{x}|^2 + \sigma^2\right), \quad (9)$$

so that we have the first order statistic  $\mathbb{E}[\bar{z}_q(n)] = 0$  and the second order statistic

$$\mathbb{E}\left[|\bar{z}_q(n)|^2\right] = P_s |h_q^{\text{SR}} + \mathbf{h}_q^{\text{TR}} \mathbf{G} \mathbf{x}|^2 + \sigma^2. \quad (10)$$

In other words,  $\mathbb{E}[\bar{z}_q(n)]$  contains no information about the transmit signal  $\mathbf{x}$ , but  $\mathbb{E}\left[|\bar{z}_q(n)|^2\right]$  has. Therefore, it implies that we should leverage  $\mathbb{E}\left[|\bar{z}_q(n)|^2\right]$  to detect the transmit signal  $\mathbf{x}$ .

### B. Averaging Process

To estimate  $\mathbb{E}\left[|\bar{z}_q(n)|^2\right]$  for detecting the transmit signal  $\mathbf{x}$ , we consider  $N$  symbols of  $\bar{z}_q(n)$ , i.e.  $\bar{z}_q(1), \bar{z}_q(2), \dots$ , and  $\bar{z}_q(N)$ , and take them as  $N$  i.i.d. samples. In other words, for each transmit signal  $\mathbf{x}$ , we use  $N$  symbols of  $\bar{z}_q(n)$  to detect it. Therefore, the Tag transmits signal  $\mathbf{x}$  with a symbol period  $T = NT_a$ , so that the symbol rate of the signal transmitted by the Tag is  $N$  times smaller than the ambient signal. Following previous methods [6], we average the power of  $\bar{z}_q(n)$  as

$$\bar{y}_q = \frac{1}{N} \sum_{n=1}^N |\bar{z}_q(n)|^2, \quad (11)$$

so as to estimate  $\mathbb{E}\left[|\bar{z}_q(n)|^2\right]$ . The resulting signal  $\bar{y}_q$  is distributed as

$$\bar{y}_q \sim \frac{P_s |h_q^{\text{SR}} + \mathbf{h}_q^{\text{TR}} \mathbf{G} \mathbf{x}|^2 + \sigma^2}{2N} \chi^2(2N), \quad (12)$$

where  $\chi^2(2N)$  refers to the chi-square distribution with  $2N$  degrees of freedom. As  $N \rightarrow \infty$ , we have  $\chi^2(2N) \xrightarrow{d} \mathcal{N}(2N, 4N)$  (normally  $N = 30$  is adequate for most applications [16], [52]), and accordingly we have

$$\bar{y}_q \sim \left(P_s |h_q^{\text{SR}} + \mathbf{h}_q^{\text{TR}} \mathbf{G} \mathbf{x}|^2 + \sigma^2\right) \mathcal{N}\left(1, \frac{1}{N}\right). \quad (13)$$

Since  $\bar{y}_q$  has mean  $P_s |h_q^{\text{SR}} + \mathbf{h}_q^{\text{TR}} \mathbf{G} \mathbf{x}|^2 + \sigma^2$ , it can be decomposed into three parts

$$\bar{y}_q = f_q(\mathbf{x}) + c_q + \bar{n}_q, \quad (14)$$

where  $f_q(\mathbf{x})$  refers to the signal and is given by

$$\begin{aligned} f_q(\mathbf{x}) &= P_s |h_q^{\text{SR}} + \mathbf{h}_q^{\text{TR}} \mathbf{G} \mathbf{x}|^2 + \sigma^2 - \left(P_s |h_q^{\text{SR}}|^2 + \sigma^2\right) \\ &= 2P_s \Re\{h_q^{\text{SR}*} \mathbf{h}_q^{\text{TR}} \mathbf{G} \mathbf{x}\} + P_s |\mathbf{h}_q^{\text{TR}} \mathbf{G} \mathbf{x}|^2. \end{aligned} \quad (15)$$

$c_q$  refers to a bias containing no information about the transmit signal and is a constant given by

$$c_q = P_s |h_q^{\text{SR}}|^2 + \sigma^2, \quad (16)$$

where  $c_q + f_q(\mathbf{x}) = P_s |h_q^{\text{SR}} + \mathbf{h}_q^{\text{TR}} \mathbf{G} \mathbf{x}|^2 + \sigma^2$ .  $\bar{n}_q$  refers to the noise given by

$$\bar{n}_q \sim \left(P_s |h_q^{\text{SR}} + \mathbf{h}_q^{\text{TR}} \mathbf{G} \mathbf{x}|^2 + \sigma^2\right) \mathcal{N}\left(0, \frac{1}{N}\right). \quad (17)$$

It is also worth noting that the received signals must be symbol-synchronized in order to determine when the Tag starts to backscatter signal. In [8], a preamble sequence is added to

the head of the bit stream. At the receiver, cross correlation of the known preamble symbol sequence and received signal is calculated. The starting point of the bit stream is defined as the point that maximizes the cross correlation.

### C. Challenges to Use AmBC Channel Model

Focusing on the previous channel model for AmBC, (14), we find that there are two challenges to use the AmBC channel model.

1) *Nonlinear Channel*: The signal  $f_q(\mathbf{x})$  is a quadratic function of  $\mathbf{x}$ , which is different from the linear function of  $\mathbf{x}$  in the conventional linear MIMO channel model. In addition, there is a constant bias  $c_q$  having no information of the transmit signal  $\mathbf{x}$ , which arises from the averaging process.

2) *Dependent Noise*: The noise  $\bar{n}_q$  has a zero mean and a variance, denoted as  $\varsigma_q^2$ , which is given by

$$\varsigma_q = \frac{P_s |h_q^{\text{SR}} + \mathbf{h}_q^{\text{TR}} \mathbf{G} \mathbf{x}|^2 + \sigma^2}{\sqrt{N}}. \quad (18)$$

We find that the variance of  $\bar{n}_q$  depends on the transmit signal  $\mathbf{x}$ , and the channels  $h_q^{\text{SR}}$ ,  $\mathbf{h}_q^{\text{TR}}$ , and  $\mathbf{G}$ , which is significantly different from the conventional AWGN.

The two challenges make the detection of transmit signal  $\mathbf{x}$  difficult and increase the detection complexity, especially for OSTBC detection as shown in Sections IV and V.

## III. AMBC CHANNEL LINEARIZATION

In this section, we propose two techniques, namely AmBC channel linearization and noise normalization, to overcome the two challenges of using the AmBC channel model (14), so that conventional approaches in MIMO communications such as OSTBC can be applied to AmBC.

### A. Linearization

The direct link (ambient RF source to Reader) has a significantly higher channel gain than the indirect link (ambient RF source to Tag and then backscattered to Reader). This corresponds to the fact that the relative SNR  $\Delta\gamma$  in practical AmBC systems is usually higher than 30 dB, which is confirmed by simulation in Section VI. Therefore, we have that

$$|\mathbf{h}_q^{\text{TR}} \mathbf{G} \mathbf{x}| \ll |h_q^{\text{SR}}|. \quad (19)$$

We rewrite  $|h_q^{\text{SR}} + \mathbf{h}_q^{\text{TR}} \mathbf{G} \mathbf{x}|^2$  as

$$\begin{aligned} &|h_q^{\text{SR}} + \mathbf{h}_q^{\text{TR}} \mathbf{G} \mathbf{x}|^2 \\ &= |h_q^{\text{SR}}|^2 \left( \left(1 + \Re\left\{\frac{\mathbf{h}_q^{\text{TR}} \mathbf{G} \mathbf{x}}{h_q^{\text{SR}}}\right\}\right)^2 + \Im\left\{\frac{\mathbf{h}_q^{\text{TR}} \mathbf{G} \mathbf{x}}{h_q^{\text{SR}}}\right\}^2 \right). \end{aligned} \quad (20)$$

From (19), we have that  $\Re\left\{\frac{\mathbf{h}_q^{\text{TR}} \mathbf{G} \mathbf{x}}{h_q^{\text{SR}}}\right\} \rightarrow 0$  and  $\Im\left\{\frac{\mathbf{h}_q^{\text{TR}} \mathbf{G} \mathbf{x}}{h_q^{\text{SR}}}\right\} \rightarrow 0$ . Subsequently, by taking the Taylor expansion of  $\left(1 + \Re\left\{\frac{\mathbf{h}_q^{\text{TR}} \mathbf{G} \mathbf{x}}{h_q^{\text{SR}}}\right\}\right)^2 + \Im\left\{\frac{\mathbf{h}_q^{\text{TR}} \mathbf{G} \mathbf{x}}{h_q^{\text{SR}}}\right\}^2$ , we can ignore the second order terms so as to approximate (20) as

$$|h_q^{\text{SR}} + \mathbf{h}_q^{\text{TR}} \mathbf{G} \mathbf{x}|^2 \approx |h_q^{\text{SR}}|^2 + 2\Re\{h_q^{\text{SR}*} \mathbf{h}_q^{\text{TR}} \mathbf{G} \mathbf{x}\}. \quad (21)$$

Therefore, according to the definition of  $f_q(\mathbf{x})$  (15), we can approximate  $f_q(\mathbf{x})$  as

$$f_q(\mathbf{x}) \approx 2P_s \Re \{ h_q^{\text{SR}*} \mathbf{h}_q^{\text{TR}} \mathbf{G} \mathbf{x} \}. \quad (22)$$

To quantify the error for omitting  $P_s |h_q^{\text{TR}} \mathbf{G} \mathbf{x}|^2$  in the information signal (15), we express its error relative to the total information signal as

$$\epsilon = \frac{\mathbb{E} [P_s |h_q^{\text{TR}} \mathbf{G} \mathbf{x}|^2]}{\mathbb{E} [2P_s \Re \{ h_q^{\text{SR}*} \mathbf{h}_q^{\text{TR}} \mathbf{G} \mathbf{x} \} + P_s |h_q^{\text{TR}} \mathbf{G} \mathbf{x}|^2]}. \quad (23)$$

It is shown in Section VI that this error is negligible.

The constant bias term  $c_q$  in the channel model (14) can also be removed. According to (14), one way to estimate  $c_q$  is to have the Tag not transmit anything in the first symbol period (equivalently the transmit signal is  $\mathbf{x} = \mathbf{0}$ ). Since  $f_q(\mathbf{0}) = 0$ , at the Reader we have that

$$\bar{y}_{q,\mathbf{x}=\mathbf{0}} = f_q(\mathbf{0}) + c_q + \bar{n}_q = c_q + \bar{n}_q. \quad (24)$$

Therefore, we can select  $\bar{y}_{q,\mathbf{x}=\mathbf{0}}$  as the estimated bias  $c_q$  since the noise term  $\bar{n}_q$  is small. This estimation approach has also been used previously [8], [16], [50], [53].

It is also important to consider the estimation errors of the bias  $c_q$ . As shown in equation (24), the estimation error is the noise term  $\bar{n}_q$ . Such estimation error will degrade detection performance in AmBC. However, from equation (17), we can minimize the estimation error by increasing the number of samples  $N$ . By using a large value of  $N$  to estimate  $c_q$ , the estimation error can be reduced. In the remainder of the paper we assume perfect estimation of  $c_q$  for simplicity.

In summary, based on the approximation (22) and removing bias  $c_q$ , the nonlinear AmBC channel can be entirely linearized.

### B. Noise Normalization

As shown in (18), the variance of the noise depends on the transmit signal  $\mathbf{x}$ , and the channels  $h_q^{\text{SR}}$ ,  $\mathbf{h}_q^{\text{TR}}$ , and  $\mathbf{G}$ . This makes the detection of  $\mathbf{x}$  difficult since 1) the noise  $\bar{n}_q$  is correlated with the transmit signal  $\mathbf{x}$ , and 2) the noise  $\bar{n}_q$  has different power levels at different Reader antennas.

To solve this difficulty, we first omit the term  $\mathbf{h}_q^{\text{TR}} \mathbf{G} \mathbf{x}$  in (18) according to (19) so that the standard deviation of the noise  $c_q$  can be approximately written as

$$c_q \approx \frac{P_s |h_q^{\text{SR}}|^2 + \sigma^2}{\sqrt{N}} = \frac{c_q}{\sqrt{N}}. \quad (25)$$

This approximation allows us to treat the noise as being uncorrelated to the transmit signal  $\mathbf{x}$ . In addition we have tested, numerically, that omitting the term  $\mathbf{h}_q^{\text{TR}} \mathbf{G} \mathbf{x}$  in (18) has nearly no impact on detection.

With (22), (25), and removing bias  $c_q$ , we can rewrite our AmBC channel model (14) as

$$\bar{y}_q - c_q = 2P_s \Re \{ h_q^{\text{SR}*} \mathbf{h}_q^{\text{TR}} \mathbf{G} \mathbf{x} \} + \frac{c_q}{\sqrt{N}} n_q. \quad (26)$$

where  $n_q \sim \mathcal{N}(0, 1)$ . However, the approximate noise (25) still has power levels dependent on  $|h_q^{\text{SR}}|^2$  at different Reader

antennas, which is still different from the conventional i.i.d. AWGN. Therefore, we normalize (26) by  $c_q/\sqrt{N}$  by defining

$$y_q = \sqrt{N} \frac{\bar{y}_q - c_q}{c_q}, \quad (27)$$

so that we have

$$y_q = \frac{2\sqrt{N}\gamma_d}{\gamma_d |h_q^{\text{SR}}|^2 + 1} \Re \{ h_q^{\text{SR}*} \mathbf{h}_q^{\text{TR}} \mathbf{G} \mathbf{x} \} + n_q. \quad (28)$$

which is now a linear channel model with i.i.d. AWGN.

In summary, by approximating  $f_q(\mathbf{x})$  (22), removing bias (24), approximating the noise (25), and normalizing the noise power (27), we can approximate the original channel model in AmBC (14) as a linear channel model with i.i.d. AWGN (28). This channel model approximation is accurate for most practical configurations in AmBC as shown later in Section VI.

### C. BPSK Modulation

In this paper, we focus on using BPSK modulation for the transmit signal  $\mathbf{x}$ , i.e.  $x_m = \pm 1$ . For BPSK modulation (or other real constellations), we can rewrite (28) in a compact form as

$$y_q = \mathbf{h}_q \mathbf{x} + n_q, \quad (29)$$

where  $\mathbf{h}_q = [h_{q,1}, h_{q,2}, \dots, h_{q,M}]$  and  $h_{q,m}$  is given by

$$h_{q,m} = 2\alpha A_{\text{TR}} \sqrt{N} \frac{\gamma_d \Re \{ h_q^{\text{SR}*} h_{q,m}^{\text{TR}} h_m^{\text{ST}} \}}{\gamma_d |h_q^{\text{SR}}|^2 + 1}. \quad (30)$$

For the proposed AmBC system with multiple-antenna Tag, the receive SNR at the Reader is given by

$$\begin{aligned} \frac{\mathbb{E} [|\mathbf{h}_q \mathbf{x}|^2]}{\mathbb{E} [n_q^2]} &= \mathbb{E} [\|\mathbf{h}_q\|^2] \\ &= \frac{4MN}{\Delta\gamma} \mathbb{E} \left[ \left( \frac{\gamma_d \Re \{ h_{1,1}^{\text{SR}*} h_{1,1}^{\text{TR}} h_1^{\text{ST}} \}}{\gamma_d |h_1^{\text{SR}}|^2 + 1} \right)^2 \right], \end{aligned} \quad (31)$$

which for all  $q$  is identical. It is important to note that using multiple antennas at the Tag can increase the receive SNR at the Reader by  $M$  times, which arises from (6). To highlight this benefit of the multiple-antenna Tag over a single-antenna Tag, we define as a reference the receive SNR for a single-antenna Tag AmBC, which is denoted as  $\gamma_R$  and given by

$$\gamma_R = \frac{4N}{\Delta\gamma} \mathbb{E} \left[ \left( \frac{\gamma_d \Re \{ h_{1,1}^{\text{SR}*} h_{1,1}^{\text{TR}} h_1^{\text{ST}} \}}{\gamma_d |h_1^{\text{SR}}|^2 + 1} \right)^2 \right]. \quad (32)$$

Accordingly, in the simulation results in Section VI, the BER performance is evaluated versus  $\gamma_R$ . When  $\gamma_d \rightarrow 0$ , we have

$$\gamma_R = \frac{4N\gamma_d^2}{\Delta\gamma} \mathbb{E} [\Re^2 \{ h_{1,1}^{\text{SR}*} h_{1,1}^{\text{TR}} h_1^{\text{ST}} \}], \quad (33)$$

which means that  $\gamma_R$  increases with  $\gamma_d$  quadratically. However, when  $\gamma_d \rightarrow \infty$ , we have

$$\gamma_R = \frac{4N}{\Delta\gamma} \mathbb{E} \left[ \Re^2 \left\{ \frac{h_{1,1}^{\text{TR}} h_1^{\text{ST}}}{h_1^{\text{SR}}} \right\} \right], \quad (34)$$

which means that  $\gamma_R$  cannot go to infinity with increasing  $\gamma_d$  and agrees with the expected result in practice.

We collect  $y_q$  for all  $q$  into  $\mathbf{y} = [y_1, y_2, \dots, y_Q]^T$ ,  $n_q$  for all  $q$  into  $\mathbf{n} = [n_1, n_2, \dots, n_Q]^T$ , and  $\mathbf{h}_q$  for all  $q$  into  $\mathbf{H} = [\mathbf{h}_1^T, \mathbf{h}_2^T, \dots, \mathbf{h}_Q^T]^T$ , so that we can construct a linearized and normalized MIMO channel model for AmBC as

$$\mathbf{y} = \mathbf{H}\mathbf{x} + \mathbf{n}. \quad (35)$$

Based on the MIMO channel model (35), we can apply conventional MIMO communication approaches to AmBC to enhance its performance. In the following sections, we apply coherent and non-coherent OSTBC to enhance the backscattered signal detection performance in AmBC.

#### IV. COHERENT OSTBC

We apply OSTBC [54] in the proposed AmBC system to enhance performance because it has a straightforward design, low decoding complexity and low power consumption. Since ambient signals are unknown, it has been an open problem to utilize OSTBC in AmBC systems [51]. By leveraging our linearized and normalized MIMO channel model (35), OSTBC can be straightforwardly applied to AmBC systems. Using OSTBC requires CSIR, but does not require CSIT so that there is no need for any feedback. The basic principle of OSTBC is that  $M$  symbols are coded across  $M$  antennas and also over  $M$  symbol periods, so that a multiplexing gain of unity is maintained. It should be noted that real orthogonal design exists if and only if  $M = 2, 4, 8$ .

##### A. Encoding Algorithm

Consider  $M$  bits ( $M = 2, 4, 8$ ),  $b_{Mi-M+1}, \dots, b_{Mi}$ , that are to be transmitted as the  $i$ th block. Using BPSK,  $b_{Mi-M+1}, \dots, b_{Mi}$  are modulated to  $M$  symbols  $u_{Mi-M+1}, \dots, u_{Mi} \in \{\pm 1\}$ . According to [54], the  $M$  symbols are encoded into a block  $\mathbf{X}_i = [\mathbf{x}_{Mi-M+1}, \mathbf{x}_{Mi-M+2}, \dots, \mathbf{x}_{Mi}]$ , where  $\mathbf{x}_{Mi}$  denotes the signals transmitted by  $M$  Tag antennas at symbol period  $Mi$  and satisfies

$$\mathbf{X}_i^T \mathbf{X}_i = (u_{Mi-M+1}^2 + \dots + u_{Mi}^2) \mathbf{I}_M, \quad (36)$$

where  $\mathbf{I}_M$  represents the  $M \times M$  identity matrix.

It terms of implementing this at the AmBC Tag, it should be noted that by tuning the load impedance of the Tag, the transmitted OSTBC symbol can be mapped to the reflection coefficient of the load impedance [5]. In addition, a low-power micro-controller on the Tag can save and process the data needed to form a block [4].

##### B. Coherent Detection

Since encoding and detecting  $\mathbf{X}_i$  do not rely on the other blocks, we simplify the analysis by only considering the first block  $\mathbf{X}_1 = [\mathbf{x}_1, \mathbf{x}_2, \dots, \mathbf{x}_M]$ . Two coherent detectors are proposed to detect the first signal vector  $\mathbf{u}_1 = [u_1, u_2, \dots, u_M]^T$ . The first detector is the optimal ML detector based on the accurate AmBC channel model (14). The second detector is a linear detector with low complexity based on the linearized

and normalized MIMO channel model (35). The two detectors are compared with each other in the numerical experiments as shown in Section VI to show the accuracy of proposed MIMO channel model.

Recall that for each transmit signal  $\mathbf{x}$ , we use  $N$  symbols of  $\bar{z}_q(n)$  to detect it through the averaging process as shown in Section II.B. Therefore, it takes  $MN$  symbols of  $\bar{z}_q(n)$  to decode the block  $\mathbf{X}_1$ . For example, as per (11),  $\bar{z}_q(1), \dots, \bar{z}_q(N)$  are used to achieve  $\bar{y}_{q,1}$  and  $\bar{z}_q((M-1)N+1), \dots, \bar{z}_q(MN)$  are used to achieve  $\bar{y}_{q,M}$ . To explicitly show the dependence on the symbol periods, we add extra subscripts for different terms such as signals and noise. For example,  $\bar{y}_{q,1}$  and  $\bar{y}_{q,M}$  denote the signal received by the  $q$ th Reader antenna at symbol periods 1 and  $M$ , respectively.

1) *Optimal ML Detector*: Based on the accurate AmBC channel model (14), we apply the optimal ML detector to detect  $\mathbf{u}_1$ . In ML detector, we maximize the posteriori probability density function (PDF),  $f(\bar{\mathbf{Y}}_1 | \mathbf{X}_1)$ , where  $\bar{\mathbf{Y}}_1$  is  $Q \times M$  matrix with the  $(q, j)$ th entry being  $\bar{y}_{q,j}$  for  $j = 1, 2, \dots, M$ . Since  $\bar{y}_{q,j}$  at different Reader antennas and different symbol periods are independent given  $\mathbf{X}_1$ , we can simplify the ML detector as

$$\tilde{\mathbf{u}}_1 = \underset{u_1, \dots, u_M \in \{\pm 1\}}{\operatorname{argmax}} \prod_{q=1}^Q \prod_{j=1}^M \frac{1}{c_{q,j}} e^{-\left| \frac{\bar{y}_{q,j} - f_q(\mathbf{x}_j) - c_q}{c_{q,j}} \right|^2}, \quad (37)$$

where we leverage the Gaussian distribution of the noise (17). It should be noted that  $c_{q,j}$  relies on  $\mathbf{x}_j$  as shown (18). The optimal ML detector is computationally intricate since it needs to compute the exponential function and it cannot separately decode  $u_1$  to  $u_M$ .

2) *Linear Detector*: To reduce the computational complexity of the optimal ML detector, we can use a linear detector to decode  $u_1$  to  $u_M$  [54], [55]. However, it is not applicable under the accurate AmBC channel model (14) because 1) the channel is nonlinear and 2) the noise is dependent on the signals and channels. To solve this problem, we leverage the linearized and normalized MIMO channel model (35) and then apply the linear detector.

Specifically, leveraging (29), we have that

$$y_{q,j} = \mathbf{h}_q \mathbf{x}_j + n_{q,j}, \quad j = 1, 2, \dots, M, \quad (38)$$

where  $y_{q,j}$  can be achieved by linearizing and normalizing  $\bar{y}_{q,j}$ , i.e.  $y_{q,j} = \sqrt{N}(\bar{y}_{q,j} - c_q)/c_q$  and  $\mathbf{h}_q$  is given by (30). According to the linear detector [54], [55], we first compute  $\mathbf{v}_q$  by  $\mathbf{v}_q = [v_{q,1}, v_{q,2}, \dots, v_{q,M}]^T = \mathbf{\Lambda}^T [y_{q,1}, y_{q,2}, \dots, y_{q,M}]^T$  where  $\mathbf{\Lambda}$  is the matrix that satisfies  $\mathbf{\Lambda} \mathbf{u}_1 = [\mathbf{h}_q \mathbf{x}_1, \mathbf{h}_q \mathbf{x}_2, \dots, \mathbf{h}_q \mathbf{x}_M]^T$ . Then we detect  $u_1$  to  $u_M$  by

$$\tilde{u}_j = \begin{cases} 1 & , \text{if } \sum_{q=1}^Q v_{q,j} \geq 0 \\ -1 & , \text{if } \sum_{q=1}^Q v_{q,j} < 0 \end{cases}, \quad j = 1, 2, \dots, M. \quad (39)$$

It should be noted that the decision statistic in (39) is simplified since BPSK modulation is used. A more general decision statistic for other modulations can be found in [54].

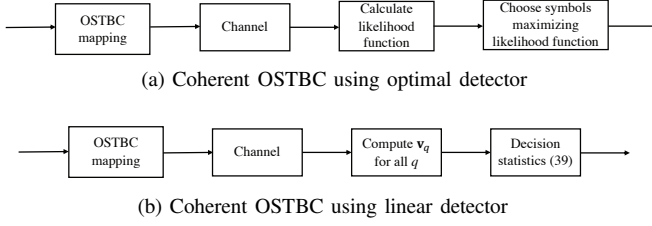


Fig. 2. Block diagrams for our proposed coherent OSTBC systems.

To conclude, leveraging the proposed linearized and normalized MIMO channel model, we can apply linear detection to separately detect  $u_1$  to  $u_M$  and avoid computing the exponential function. Therefore the computational complexity for detection is greatly reduced. The block diagrams for coherent OSTBC using optimal and linear detectors are shown in Fig. 2.

3) *Equivalence*: It is worthwhile to show the approximate equivalence between the optimal ML detector based on (14) and the linear detector based on (35).

Using the approximated noise (25), we can simplify (37) as

$$\tilde{\mathbf{u}}_1 = \underset{u_1, \dots, u_M \in \{\pm 1\}}{\operatorname{argmin}} \sum_{q=1}^Q \sum_{j=1}^M \left| \sqrt{N} \frac{\bar{y}_{q,j} - f_q(\mathbf{x}_j) - c_q}{c_q} \right|^2. \quad (40)$$

Using the channel linearization and the noise normalization, we can further simplify (40) as

$$\tilde{\mathbf{u}}_1 = \underset{u_1, \dots, u_M \in \{\pm 1\}}{\operatorname{argmin}} \sum_{q=1}^Q \sum_{j=1}^M |y_{q,j} - \mathbf{h}_q \mathbf{x}_j|^2, \quad (41)$$

which is a minimum distance detector [56]. As shown previously [54], [55], the minimum distance detector (41) is equivalent to the linear detector (39).

It can be concluded that using the linear detector with the linearized and normalized MIMO channel model (35) is equivalent to the optimal ML detector with the accurate AmBC channel model (14). A numerical comparison for those two detectors is provided in Section VI to verify the equivalence.

### C. BER Analysis

Leveraging the linearized and normalized MIMO channel (35), we also provide a BER analysis for the coherent OSTBC with BPSK.

1) *Single-Antenna Tag Single-Antenna Reader*: We first consider the conventional SISO (i.e.  $M = 1$  and  $Q = 1$ ) AmBC system using BPSK as a comparison. Using (29), we have that

$$y_1 = 2\alpha A_{\text{TR}} \sqrt{N} \gamma_d \frac{\Re \{h_1^{\text{SR}*} h_{1,1}^{\text{TR}} h_1^{\text{ST}}\}}{\gamma_d |h_1^{\text{SR}}|^2 + 1} x_1 + n_1. \quad (42)$$

Given the channel realizations  $h_1^{\text{SR}}$ ,  $h_1^{\text{ST}}$ , and  $h_{1,1}^{\text{TR}}$ , it is straightforward to derive the BER for the SISO AmBC as

$$P_{\text{SISO}} = Q \left( 2\alpha A_{\text{TR}} \sqrt{N} \gamma_d \left| \frac{\Re \{h_1^{\text{SR}*} h_{1,1}^{\text{TR}} h_1^{\text{ST}}\}}{\gamma_d |h_1^{\text{SR}}|^2 + 1} \right| \right). \quad (43)$$

2) *Multiple-Antenna Tag Multiple-Antenna Reader*: For the multiple-antenna Tag multiple-antenna Reader AmBC system, we start by noting that  $\sum_{q=1}^Q v_{q,1}$  given  $u_1$  is distributed as  $\sum_{q=1}^Q v_{q,1} \sim \mathcal{N} \left( u_1 \sum_{q=1}^Q \|\mathbf{h}_q\|^2, \sum_{q=1}^Q \|\mathbf{h}_q\|^2 \right)$ . Given the channel realizations  $\mathbf{h}_q$ , from (39), it is straightforward to derive that the BER of AmBC using the linear detector with BPSK is given by

$$P_{\text{Linear}} = Q \left( 2\alpha A_{\text{TR}} \sqrt{N} \gamma_d \sqrt{\sum_{q=1}^Q \sum_{m=1}^M \left| \frac{\Re \{h_q^{\text{SR}*} h_{q,m}^{\text{TR}} h_m^{\text{ST}}\}}{\gamma_d |h_q^{\text{SR}}|^2 + 1} \right|^2} \right). \quad (44)$$

Therefore, we can deduce that using multiple-antenna Tag and multiple-antenna Reader can effectively decrease the BER compared with conventional SISO AmBC. The BERs of the MIMO AmBC and the SISO AmBC are numerically compared in Section VI.

## V. NON-COHERENT OSTBC

The limitation of coherent OSTBC is that it requires CSI at the Reader. Although methods have been demonstrated that provide CSI in AmBC [57]-[62], estimating the channel is not desirable in AmBC. For example a blind channel estimation method based on expectation maximization (EM)-based estimator [57], [58], has been proposed to obtain CSI. While it is effective, the channel estimation process inevitably increases the complexity of AmBC system design as well as power consumption and it is therefore useful to consider methods that do not need CSI [16].

We propose using non-coherent differential OSTBC to remove the need for CSI. Differential OSTBC is a transmission scheme for exploiting diversity given by multiple antennas when neither the transmitter nor the receiver requires CSI. The scheme has a straightforward encoding design and low decoding complexity, which can provide full spatial diversity and requires no CSI [63], [64]. In this section we restrict the formulation to 2-port Tag antennas, for clarity of explanation, so that  $M = 2$  but the method can be applied to  $M = 2, 4, 8$  similarly to coherent OSTBC.

### A. Encoding Algorithm

In differential OSTBC [63], [64], the Tag transmits the signal as blocks. The two bits  $b_{2i-1}$  and  $b_{2i}$  are mapped to two symbols  $u_{2i-1}, u_{2i} \in \{\pm 1\}$ , which are then encoded into the  $i$ th block  $\mathbf{X}_i$  as shown in (36).

The Tag begins the transmission by sending the first block  $\mathbf{X}_1$  where  $u_1$  and  $u_2$  are arbitrary symbols. The symbols  $u_1$  and  $u_2$  are unknown to the Reader and do not convey any information. The Tag subsequently transmits the signal block in an inductive manner. Supposing  $\mathbf{X}_i$  has been sent already, to transmit the next block  $\mathbf{X}_{i+1}$ , we need to map  $b_{2i+1}$  and  $b_{2i+2}$  to symbols  $u_{2i+1}$  and  $u_{2i+2}$ . This mapping depends on  $\mathbf{X}_i$ , which is different from coherent OSTBC where  $\mathbf{X}_i$

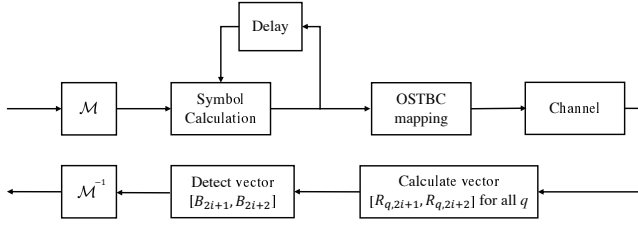


Fig. 3. Block diagram for our proposed non-coherent OSTBC systems.

and  $\mathbf{X}_{i+1}$  are independent of each other. Specifically, we first use a mapping  $\mathcal{M}$  to map  $b_{2i+1}$  and  $b_{2i+2}$  to a vector  $[B_{2i+1}, B_{2i+2}]$ , i.e.  $\mathcal{M}(b_{2i+1}, b_{2i+2}) = [B_{2i+1}, B_{2i+2}]$  where the mapping is given by [63],

$$\begin{aligned} \mathcal{M}(0, 0) &= [1, 0], & \mathcal{M}(0, 1) &= [0, -1] \\ \mathcal{M}(1, 0) &= [0, 1], & \mathcal{M}(1, 1) &= [-1, 0] \end{aligned} \quad (45)$$

The two symbols  $u_{2i+1}$  and  $u_{2i+2}$  are then computed by

$$\begin{bmatrix} u_{2i+1} \\ u_{2i+2} \end{bmatrix} = B_{2i+1} \begin{bmatrix} u_{2i-1} \\ u_{2i} \end{bmatrix} + B_{2i+2} \begin{bmatrix} -u_{2i} \\ u_{2i-1} \end{bmatrix}. \quad (46)$$

Finally, the two symbols  $u_{2i+1}$  and  $u_{2i+2}$  are encoded into the block  $\mathbf{X}_{i+1}$  as shown in (36). This process is inductively repeated until the end of the transmission.

### B. Non-Coherent Detection

For the non-coherent detector, it is not possible to use the accurate AmBC channel model (14) because of 1) the channel is nonlinear, and 2) the noise is dependent on the signals and channels. Therefore, we again leverage the linearized and normalized MIMO channel model (35) and apply the differential OSTBC detector [63].

Using the differential OSTBC detector, we first detect the vector  $[B_{2i+1}, B_{2i+2}]$

$$\begin{aligned} [\tilde{B}_{2i+1}, \tilde{B}_{2i+2}] &= \underset{[B_{2i+1}, B_{2i+2}] \in \mathcal{V}}{\operatorname{argmin}} \sum_{q=1}^Q \|[B_{2i+1}, B_{2i+2}] \\ &\quad - [\mathcal{R}_{q,2i+1}, \mathcal{R}_{q,2i+2}]\|^2, \end{aligned} \quad (47)$$

where  $\mathcal{V}$  denotes the set consisting all the vectors  $[B_{2i+1}, B_{2i+2}]$  and  $\mathcal{R}_{q,2i+1}$  and  $\mathcal{R}_{q,2i+2}$  are

$$\mathcal{R}_{q,2i+1} = y_{q,2i+1}y_{q,2i-1} + y_{q,2i+2}y_{q,2i}, \quad (48)$$

$$\mathcal{R}_{q,2i+2} = y_{q,2i+1}y_{q,2i} - y_{q,2i+2}y_{q,2i-1}, \quad (49)$$

where  $y_{q,2i-1}$ ,  $y_{q,2i}$ ,  $y_{q,2i+1}$ , and  $y_{q,2i+2}$  denote the signals received by the Reader at four consecutive symbol periods  $2i-1$ ,  $2i$ ,  $2i+1$ ,  $2i+2$ . We can then detect the two bits  $b_{2i+1}$  and  $b_{2i+2}$  from  $[B_{2i+1}, B_{2i+2}]$  since they have one-to-one correspondence. The block diagram of the differential OSTBC system can be found in Fig. 3.

## VI. SIMULATION RESULTS

We provide simulation results for the proposed AmBC system using coherent and non-coherent OSTBC. A conventional SISO AmBC system ( $M = 1$ ,  $Q = 1$ ) using coherent detection [13] and two SISO AmBC systems using differential detectors [15], [16] are also simulated as benchmarks for comparison. In the simulation, we assume all the small-scale channel fading  $h_q^{\text{SR}}$ ,  $h_q^{\text{TR}}$  and  $h_q^{\text{ST}}$  are distributed as  $\mathcal{CN}(0, 1)$ . The hardware implementation loss by the Tag,  $\alpha$ , is set as 1.1 dB [11]. The Monte Carlo method is used to find the BER.

In the simulation results we focus on the configuration in which the number of Tag antennas is  $M = 2$ . This ensures a multiplexing factor of unity (so as not sacrifice throughput) as well as allowing the Tag to be compact. Compact 2-port Tag antennas can be easily found [65], [66] but for  $M > 2$  multi-port antenna designs with the same density of antennas (in terms of ports per square or cubic wavelength) are not as straightforward to produce. We also provide limited results for  $M > 2$  to demonstrate the versatility of the proposed method as well as the limitations of the proposed linear AmBC MIMO channel model.

### A. Coherent OSTBC

For the proposed AmBC system, we simulate the BER versus receive SNR  $\gamma_R$  by using the optimal ML detector (37) and the linear detector (39). For the SISO AmBC system, we simulate the BER by using the optimal ML detector previously proposed [13] and the minimum distance detector [56] based on the linearized and normalized channel. The simulated BERs of the MIMO AmBC system using OSTBC and the SISO AmBC system using BPSK for the relative SNR  $\Delta\gamma = 40$  dB and the direct link SNR  $\gamma_d = 15$  dB, which are practical values, are shown in Fig. 4. Recall that the relative SNR  $\Delta\gamma$  depends on the hardware implementation loss  $\alpha$  and path loss  $A_{\text{TR}}$  while the direct link SNR  $\gamma_d$  is  $P_s/\sigma^2$ . Besides,  $\gamma_R$  depends on  $\Delta\gamma$ ,  $\gamma_d$ ,  $N$ , and the channels as shown in (32). We use (43) and (44) to calculate the theoretical BER for a given channel realization. Using Monte Carlo method, we generate multiple independent channel realizations and average the obtained theoretical BERs. The averaged BER results are denoted as theoretical analysis and included in Fig. 4 as a reference.

In Fig. 4, five configurations are shown:  $1 \times 1$ ,  $2 \times 1$ ,  $2 \times 2$ ,  $4 \times 2$  and  $8 \times 2$ . In terms of approximation accuracy, comparing the five groups of curves, three key observations can be highlighted.

*First*, from Fig. 4(a) and (b), when  $M = 1, 2$ , the optimal ML detector has almost the same BER performance as the linear detector or the minimum distance detector, which shows that our proposed linearized and normalized MIMO channel (35) well approximates the accurate AmBC channel (14). The linear detector based on the proposed channel model however has a much lower computational complexity than the optimal ML detector. Therefore, it is beneficial to use our proposed linearized and normalized MIMO channel. It can be seen that the BER performance of the linear or minimum distance



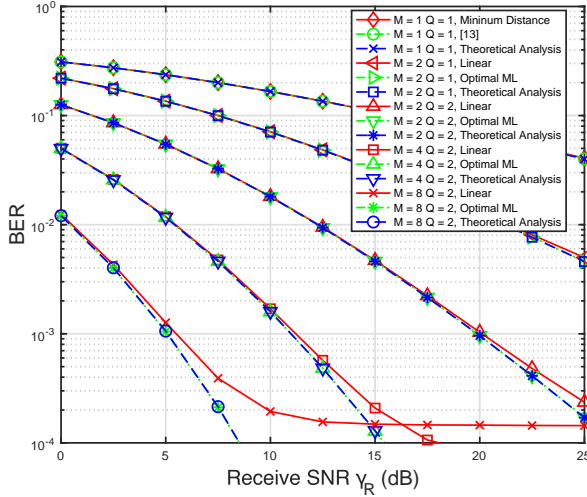
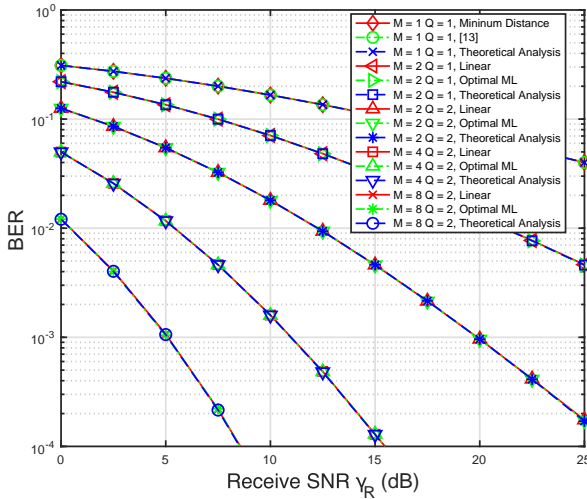
(a)  $\Delta\gamma = 40$  dB(b)  $\Delta\gamma = 50$  dB

Fig. 4. Simulated BERs versus receive SNR  $\gamma_R$  of the proposed AmBC system using the OSTBC and the SISO AmBC system using BPSK for  $\gamma_d = 15$  dB at (a)  $\Delta\gamma = 40$  dB and (b)  $\Delta\gamma = 50$  dB.

detector matches well with the theoretical analysis results (43) and (44), which validates the correctness of the analysis.

*Second*, from Fig. 4(a), when  $M = 4$ , the performance gap becomes a bit larger and when  $M = 8$ , the performance gap is obvious and there is an error floor, which indicates that the BER cannot decrease with the SNR without a limitation. Our approximation does not work well in these cases. The error floor is due to the approximation of the signal to a linear function by omitting the quadratic term  $P_s |\mathbf{h}_q^{\text{TR}} \mathbf{G} \mathbf{x}|^2$ . When increasing the antenna number, the omitted term  $P_s |\mathbf{h}_q^{\text{TR}} \mathbf{G} \mathbf{x}|^2$  causes higher error and affects the accuracy in the minimum distance detector so that it causes an error floor.

*Third*, comparing Fig. 4(a) with (b), we can find that the performance gap between the optimal ML detector and the linear detector is eliminated for  $M = 1, 2, 4, 8$  when  $\Delta\gamma$  increases from 40 to 50 dB, which shows that higher  $\Delta\gamma$  makes the approximations more accurate even for larger Tag

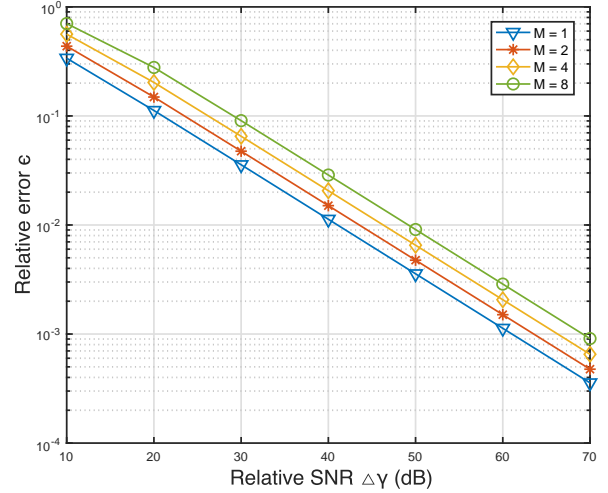


Fig. 5. The relative error for omitting  $P_s |\mathbf{h}_q^{\text{TR}} \mathbf{G} \mathbf{x}|^2$  in the information signal versus  $\Delta\gamma$  with different number of antennas

antenna numbers. In addition,  $\Delta\gamma$  increases with the distance between Tag and Reader, as will be shown in the following. In other words, as we increase the distance between Tag and Reader, our proposed approximations become more accurate even for more Tag antennas.

In summary we can conclude, that our proposed channel model approximations becomes less accurate when we increase the number of antennas and on the contrary become more accurate when we increase  $\Delta\gamma$  or equivalently the distance between Tag and Reader.

Fig. 5 shows the relative error ratio  $\epsilon$  (23) for omitting  $P_s |\mathbf{h}_q^{\text{TR}} \mathbf{G} \mathbf{x}|^2$  in the information signal versus  $\Delta\gamma$  with different number of antennas. We can find that the relative error increases with the Tag antenna number and decreases with  $\Delta\gamma$ , which agrees well with the above results.

To conclude, at  $\Delta\gamma = 40$  dB, our channel model approximation is accurate for small numbers of Tag antennas ( $M \leq 2$ ) which satisfies the size constraint for practical Tag configurations. If we extend the communication distance between the Tag and Reader to increase the relative SNR e.g.,  $\Delta\gamma = 50$  dB, the approximation can be more accurate even for more Tag antennas such as  $M = 4, 8$ . Furthermore, to emphasize the benefits of implementing multiple antennas at the Tag as well as Reader two advantages need to be highlighted:

*First*, it is important to note that the total transmit power in the MIMO AmBC system linearly increases with  $M$ , which is different from conventional MIMO communication where the total transmit power is fixed. If we set the transmit symbols as  $u_{Mi-M+1}, \dots, u_{Mi} \in \{\pm 1/\sqrt{M}\}$  as adopted in the conventional MIMO system, the BER curves for  $M = 2, 4, 8$  in Fig. 4 will right shift by  $10\lg M$  dB. Therefore, using more Tag antennas has the benefit of power gain, which effectively increases the power of the backscattered signal so as to decrease the BER, and this is unique in the AmBC setting.

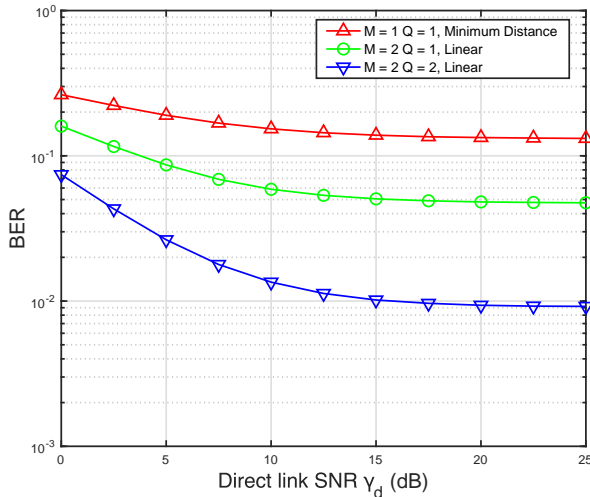


Fig. 6. Simulated BERs versus direct link SNR  $\gamma_d$  of the proposed AmBC system using coherent OSTBC and the SISO AmBC system using BPSK for  $\Delta\gamma = 40$  dB and  $N = 40000$ .

Second, comparing the BER curves of  $M = 1, Q = 1$  and  $M = 2, Q = 1$ , we can find that the slope of the BER curve is doubled by using two Tag antennas. The enhanced signal detection performance arises from leveraging the Tag diversity gain. Furthermore, comparing the BER curves of  $M = 2, Q = 1$  and  $M = 2, Q = 2$ , we can find that the slope of the BER curve is doubled by using two Reader antennas. The enhanced signal detection performance arises from leveraging the Reader diversity gain. Overall, compared with our benchmark [13], our proposed approach shows the benefit of using OSTBC in the multiple-antenna Tag multiple-antenna Reader AmBC system to enhance the signal detection performance. More generally, a diversity gain of  $MQ$  can be achieved by using more Tag/Reader antennas in AmBC.

We also study the effect of direct link SNR  $\gamma_d$  on the BER performance of the MIMO AmBC system and the SISO AmBC system. The simulated BERs versus  $\gamma_d$  are shown in Fig. 6. We only consider using the linear detector and the minimum distance detector since they have almost the same BERs as the optimal ML detector. From Fig. 6, we can observe that the BERs decrease with  $\gamma_d$  at fixed  $N = 40000$  for the three configurations. This is because the receive SNR  $\gamma_R$  increases with  $\gamma_d$ . Therefore, high  $\gamma_d$  is beneficial for AmBC to decrease the BER. However, BER cannot be decreased without limit by simply increasing  $\gamma_d$ . As shown in Fig. 6, the BERs saturate when  $\gamma_d$  is large for the three configurations. This is because when  $\gamma_d \rightarrow \infty$ ,  $\gamma_R$  saturates to  $\frac{4N}{\Delta\gamma} \mathbb{E} [\Re^2 \{h_{1,1}^{\text{TR}} h_{1,1}^{\text{ST}} / h_{1,1}^{\text{SR}}\}]$  as shown in Section III.C. In addition, we can observe that using more Tag/Reader antennas can decrease the BER given the same  $\gamma_d$ , which again shows the benefit of multiple Tag/Reader antennas.

Because our proposed linearized and normalized MIMO channel (35) is based on the relative SNR  $\Delta\gamma$  being high in AmBC, we study the effect of  $\Delta\gamma$  on the BER performance. The simulated BERs versus  $\Delta\gamma$  of the proposed AmBC ( $M = 2, Q = 1$ ) at the receive SNRs  $\gamma_R = 5, 10, 15$  dB

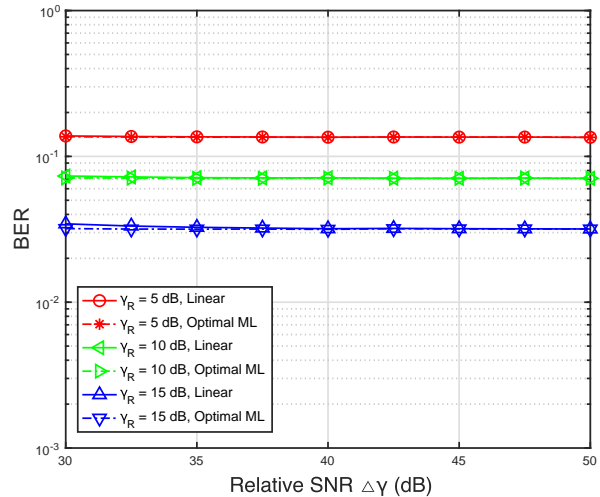


Fig. 7. Simulated BERs versus relative SNR  $\Delta\gamma$  of the proposed AmBC system using coherent OSTBC for  $M = 2, Q = 1$  at the receive SNRs  $\gamma_R = 5, 10, 15$  dB.

are shown in Fig. 7. From Fig. 7, we can observe that given a fixed  $\gamma_R$ , the optimal ML detector and the linear detector have almost the same BERs which do not change with  $\Delta\gamma$  when  $\Delta\gamma$  is larger than 35 dB. However, when  $\Delta\gamma$  is small, e.g. at 30 dB, there is a small BER performance gap between the optimal ML detector and the linear detector, which implies that the linearized and normalized MIMO channel model has some approximation error. Fortunately,  $\Delta\gamma$  in AmBC is usually higher than 30 dB.

The relative SNR  $\Delta\gamma$  has a one-to-one correspondence with the path loss since  $\Delta\gamma = 1/\alpha^2 A_{\text{TR}}^2$ . Therefore to show the range of  $\Delta\gamma$ , we use the Friis equation [56] to estimate the path loss for the ambient RF signals from different wireless systems. The path loss versus the transmission distance between the Tag and Reader for the ambient RF signals of different wireless systems is shown in Fig. 8 when we use a path-loss exponent of two. We consider common ambient RF signals from wireless systems including GSM-900 (925-960 MHz), GSM-1800 (1.805-1.88 GHz), UMTS-2100 (2.11-2.17 GHz) and WiFi (2.4-2.48 GHz), which have been well exploited for ambient RF energy harvesting [67], [68]. It should be noted that in Fig. 8, the path loss decreases with the transmission distance and it is below  $-30$  dB when the transmission distance is larger than 1 meter for all considered ambient RF signals. In other words,  $\Delta\gamma$  is at least greater than 30 dB when the Tag and Reader are separated by 1 meter or more. In previous simulations, we set  $\Delta\gamma = 40$  dB so the communication distance between Tag and Reader is around 1-2 meter, which is a practical set up. Since Fig. 7 shows that our proposed linearized and normalized MIMO channel model is accurate when the relative SNR  $\Delta\gamma$  is larger than 30 dB, or equivalently the distance between the Tag and Reader is longer than 1 meter, the proposed channel model is shown valid for practical AmBC system configurations and based on that the linear detector provides the optimal BER performance ( $M \leq 2$ ).

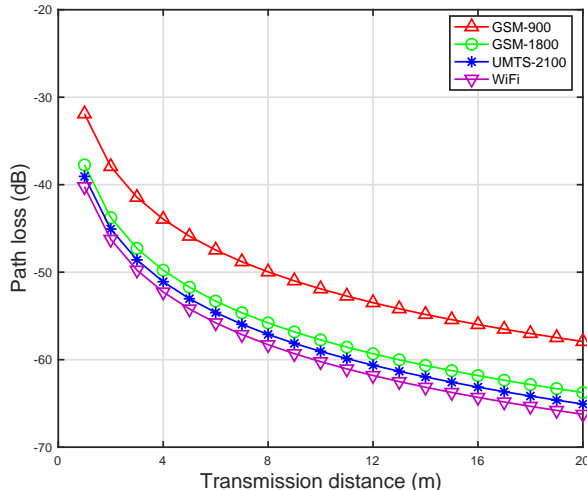


Fig. 8. Path loss versus transmission distance between the Tag and Reader for ambient RF signals from different wireless systems.

### B. Non-Coherent OSTBC

For the MIMO AmBC system, we simulate the BER by using the differential OSTBC detector (47). For the SISO AmBC system, we reproduce the methods previously proposed [15], [16] which also implement differential codes in an AmBC system.

The simulated BERs of the proposed AmBC system using our differential OSTBC and the SISO AmBC system benchmark with relative SNR  $\Delta\gamma = 40$  dB and direct link SNR  $\gamma_d = 15$  dB are shown in Fig. 9. Comparing Fig. 4 with Fig. 9, we can make three key observations.

*First*, compared with coherent OSTBC, using differential OSTBC can achieve the same slope in BER, but there is a constant BER performance loss, which results from not requiring any CSI. For SISO AmBC, there is also a constant BER loss between the minimum distance detector in BPSK and differential detector previously proposed [15], [16] for the same reason. It can also be observed that the performance loss between minimum distance detector in BPSK and [16] is the same as  $M = 2, Q = 1$ , and  $M = 2, Q = 2$  cases while the gap between minimum distance detector in BPSK and [15] is larger than other cases. The reason is that some information is lost during energy subtraction [15].

*Second*, similar to the coherent case, using more Tag antennas has the benefit of power gain, which can effectively increase the power of the backscattered signal so as to decrease the BER.

*Third*, comparing the BER curves of  $M = 1, Q = 1$ ,  $M = 2, Q = 1$ , and  $M = 2, Q = 2$ , we find that the slope of the BER curve can be doubled by using two Tag antennas or Reader antennas. Therefore, using differential OSTBC can leverage the Tag/Reader diversity gain and enhance the signal detection performance without the requirement of any CSI.

Similar to the coherent case, we also show how the direct link SNR  $\gamma_d$  and the relative SNR  $\Delta\gamma$  affect the BER performance of the proposed AmBC system using differential

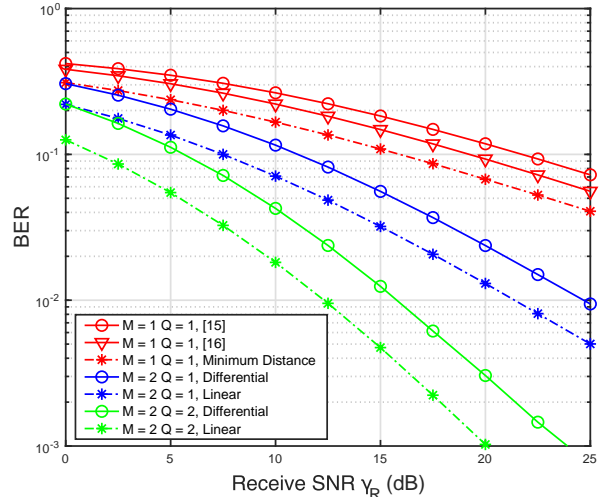


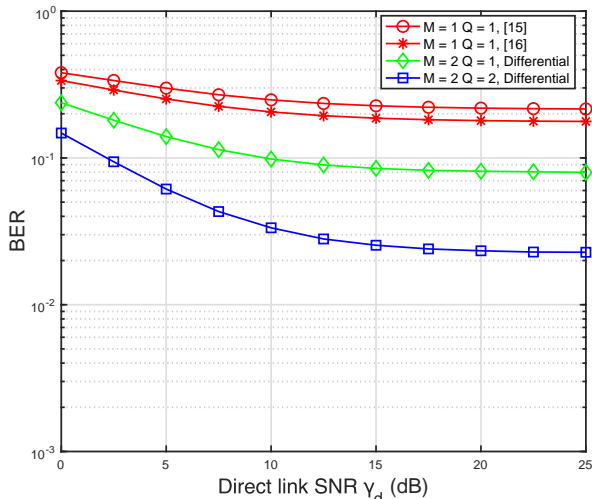
Fig. 9. Simulated BERs versus receive SNR  $\gamma_R$  of the proposed AmBC system using the differential OSTBC and the SISO AmBC system using 2DPSK for  $\Delta\gamma = 40$  dB and  $\gamma_d = 15$  dB.

OSTBC as shown in Fig. 10(a) and Fig. 10(b), respectively. We can also make observations that are similar to the case of using coherent OSTBC, and these are summarized as 1) BERs decrease with  $\gamma_d$  and saturate to a constant when  $\gamma_d \rightarrow \infty$ ; 2) BERs do not change with  $\Delta\gamma$  given a fixed  $\gamma_R$  when  $\Delta\gamma$  is larger than 35 dB, and the BERs have little increase when  $\Delta\gamma$  is at around 30 dB. The only difference between the coherent and non-coherent cases is that there is a constant BER performance loss by using differential OSTBC. However it comes at the advantage of not requiring any CSI.

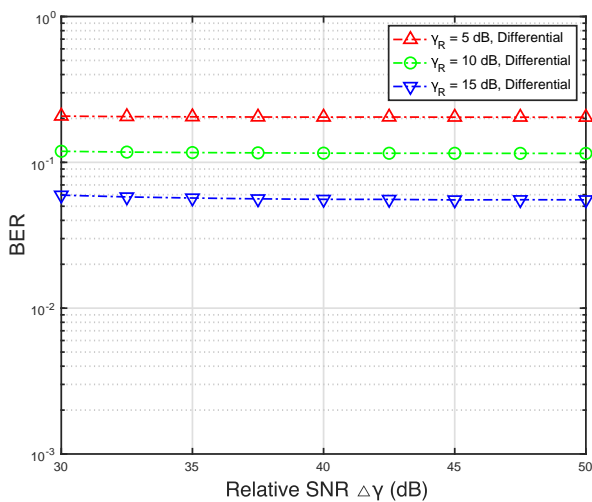
## VII. CONCLUSION

We have proposed the use of multiple-antenna Tag and multiple-antenna Reader in AmBC systems by applying coherent and non-coherent OSTBC to leverage both diversity and power gain. Both codes do not require CSIT and the non-coherent OSTBC do not require CSIR either. The multiple-antenna Tag linearly increases (linear with the number of Tag antennas) the total backscattered signal power and this is different from conventional MIMO where transmit power is fixed. Furthermore, the proposed approach is compatible with using multiple-antenna Reader to further improve diversity gain.

We have also derived an accurate channel model for the AmBC system with a multiple-antenna Tag and a multiple-antenna Reader by using the averaging mechanism. The accurate AmBC channel model is challenging to use since it is nonlinear with noise that is dependent on the signals and the channels and cannot be used with OSTBC. To overcome the challenges of using the accurate AmBC channel model, we have proposed a linearized and normalized MIMO channel model. The channel model is accurate when there are two antennas at the Tag but becomes less accurate when the number of antennas is increased. On the contrary the model becomes more accurate when  $\Delta\gamma$  is increased or equivalently the distance between Tag and Reader is increased.



(a)



(b)

Fig. 10. (a) Simulated BERs versus direct link SNR  $\gamma_d$  of the proposed AmBC system using differential OSTBC and the SISO AmBC system [15], [16] for  $\Delta\gamma = 40$  dB and  $N = 40000$ . (b) Simulated BERs versus relative SNR  $\Delta\gamma$  of the proposed AmBC system using differential OSTBC for  $M = 2$ ,  $Q = 1$  at the receive SNRs  $\gamma_R = 5, 10, 15$  dB.

Two coherent detectors, the optimal ML detector and the linear detector have been investigated and a closed-form solution for the BER was also provided. In addition a non-coherent detector based on differential OSTBC is also investigated. Using this there is no need for CSI and the AmBC system design complexity and power consumption can be reduced. The corresponding differential OSTBC detector based on the linearized and normalized MIMO channel was also provided.

Simulation results demonstrate that the proposed MIMO AmBC system using coherent and non-coherent OSTBC has performance better than the conventional SISO AmBC system. The simulation results show that using multiple Tag antennas can increase the total power of the backscattered signal. It is also shown that using OSTBC and differential OSTBC in the proposed AmBC system can effectively enhance BER performance compared compared with SISO AmBC systems.

## REFERENCES

- [1] H. Stockman, "Communication by means of reflected power," *Proc. IRE*, vol. 36, no. 10, pp. 1196–1204, 1948.
- [2] J. Landt, "The history of RFID," *IEEE Potentials*, vol. 24, no. 4, pp. 8–11, 2005.
- [3] J. Kimionis, A. Bletsas, and J. N. Sahalos, "Bistatic backscatter radio for power-limited sensor networks," in *2013 IEEE Global Communications Conference (GLOBECOM)*, 2013, pp. 353–358.
- [4] C. Boyer and S. Roy, "Backscatter communication and RFID: Coding, energy, and MIMO analysis," *IEEE Trans. Commun.*, vol. 62, no. 3, pp. 770–785, 2014.
- [5] N. Van Huynh, D. T. Hoang, X. Lu, D. Niyato, P. Wang, and D. I. Kim, "Ambient backscatter communications: A contemporary survey," *IEEE Communications Surveys Tutorials*, vol. 20, no. 4, pp. 2889–2922, 2018.
- [6] V. Liu, A. Parks, V. Talla, S. Gollakota, D. Wetherall, and J. R. Smith, "Ambient backscatter: Wireless communication out of thin air," *ACM SIGCOMM Computer Communication Review*, vol. 43, no. 4, pp. 39–50, 2013.
- [7] A. Wang, V. Iyer, V. Talla, J. R. Smith, and S. Gollakota, "FM backscatter: Enabling connected cities and smart fabrics," in *14th USENIX Symposium on Networked Systems Design and Implementation (NSDI 17)*. Boston, MA: USENIX Association, Mar. 2017, pp. 243–258. [Online]. Available: <https://www.usenix.org/conference/nsdi17/technical-sessions/presentation/wang-anran>
- [8] S. N. Daskalakis, J. Kimionis, A. Collado, G. Goussetis, M. M. Tentzeris, and A. Georgiadis, "Ambient backscatterers using FM broadcasting for low cost and low power wireless applications," *IEEE Trans. Microw. Theory Techn.*, vol. 65, no. 12, pp. 5251–5262, 2017.
- [9] B. Kellogg, A. Parks, S. Gollakota, J. R. Smith, and D. Wetherall, "Wi-Fi backscatter: Internet connectivity for rf-powered devices," in *Proceedings of the 2014 ACM Conference on SIGCOMM*, 2014, pp. 607–618.
- [10] D. Bharadia, K. R. Joshi, M. Kotaru, and S. Katti, "Backfi: High throughput WiFi backscatter," *ACM SIGCOMM Computer Communication Review*, vol. 45, no. 4, pp. 283–296, 2015.
- [11] B. Kellogg, V. Talla, S. Gollakota, and J. R. Smith, "Passive Wi-Fi: Bringing low power to Wi-Fi transmissions," in *13th USENIX Symposium on Networked Systems Design and Implementation (NSDI 16)*. Santa Clara, CA: USENIX Association, Mar. 2016, pp. 151–164. [Online]. Available: <https://www.usenix.org/conference/nsdi16/technical-sessions/presentation/kellogg>
- [12] B. Ji, B. Xing, K. Song, C. Li, H. Wen, and L. Yang, "The efficient BackFi transmission design in ambient backscatter communication systems for IoT," *IEEE Access*, vol. 7, pp. 31 397–31 408, 2019.
- [13] K. Lu, G. Wang, F. Qu, and Z. Zhong, "Signal detection and ber analysis for RF-powered devices utilizing ambient backscatter," in *2015 International Conference on Wireless Communications Signal Processing (WCSP)*, 2015, pp. 1–5.
- [14] J. K. Devineni and H. S. Dhillon, "Ambient backscatter systems: Exact average bit error rate under fading channels," *IEEE Transactions on Green Communications and Networking*, vol. 3, no. 1, pp. 11–25, 2019.
- [15] G. Wang, F. Gao, R. Fan, and C. Tellambura, "Ambient backscatter communication systems: Detection and performance analysis," *IEEE Trans. Commun.*, vol. 64, no. 11, pp. 4836–4846, 2016.
- [16] J. Qian, F. Gao, G. Wang, S. Jin, and H. Zhu, "Noncoherent detections for ambient backscatter system," *IEEE Trans. Wireless Commun.*, vol. 16, no. 3, pp. 1412–1422, 2017.
- [17] J. Qian, A. N. Parks, J. R. Smith, F. Gao, and S. Jin, "IoT communications with  $M$ -PSK modulated ambient backscatter: Algorithm, analysis, and implementation," *IEEE Internet Things J.*, vol. 6, no. 1, pp. 844–855, 2019.
- [18] Q. Tao, C. Zhong, K. Huang, X. Chen, and Z. Zhang, "Ambient backscatter communication systems with MFSK modulation," *IEEE Trans. Wireless Commun.*, vol. 18, no. 5, pp. 2553–2564, 2019.
- [19] G. Vougioukas and A. Bletsas, "Switching frequency techniques for universal ambient backscatter networking," *IEEE J. Sel. Areas Commun.*, vol. 37, no. 2, pp. 464–477, 2019.
- [20] J. Choi, "Matched-filter-based backscatter communication for IoT devices over ambient OFDM carrier," *IEEE Internet Things J.*, vol. 6, no. 6, pp. 10 229–10 239, 2019.
- [21] Y. Liu, G. Wang, Z. Dou, and Z. Zhong, "Coding and detection schemes for ambient backscatter communication systems," *IEEE Access*, vol. 5, pp. 4947–4953, 2017.
- [22] Q. Tao, C. Zhong, H. Lin, and Z. Zhang, "Symbol detection of ambient backscatter systems with Manchester coding," *IEEE Trans. Wireless Commun.*, vol. 17, no. 6, pp. 4028–4038, 2018.

- [23] G. Yang, D. Yuan, Y. Liang, R. Zhang, and V. C. M. Leung, "Optimal resource allocation in full-duplex ambient backscatter communication networks for wireless-powered IoT," *IEEE Internet Things J.*, vol. 6, no. 2, pp. 2612–2625, 2019.
- [24] X. Liu, Y. Gao, and F. Hu, "Optimal time scheduling scheme for wireless powered ambient backscatter communications in IoT networks," *IEEE Internet Things J.*, vol. 6, no. 2, pp. 2264–2272, 2019.
- [25] Z. Ma, C. He, Y. Rao, J. Jiang, S. Ma, F. Gao, and L. Xing, "Time- and power-splitting strategies for ambient backscatter system," *IEEE Access*, vol. 7, pp. 40068–40077, 2019.
- [26] L. Shi, R. Q. Hu, Y. Ye, and H. Zhang, "Modeling and performance analysis for ambient backscattering underlying cellular networks," *IEEE Trans. Veh. Technol.*, vol. 69, no. 6, pp. 6563–6577, 2020.
- [27] D. Darsena, G. Gelli, and F. Verde, "Modeling and performance analysis of wireless networks with ambient backscatter devices," *IEEE Trans. Commun.*, vol. 65, no. 4, pp. 1797–1814, 2017.
- [28] S. Zhou, W. Xu, K. Wang, C. Pan, M. Alouini, and A. Nallanathan, "Ergodic rate analysis of cooperative ambient backscatter communication," *IEEE Wireless Commun. Lett.*, vol. 8, no. 6, pp. 1679–1682, 2019.
- [29] H. Ding, D. B. da Costa, and J. Ge, "Outage analysis for cooperative ambient backscatter systems," *IEEE Wireless Commun. Lett.*, vol. 9, no. 5, pp. 601–605, 2020.
- [30] Y. Ye, L. Shi, X. Chu, and G. Lu, "On the outage performance of ambient backscatter communications," *IEEE Internet Things J.*, vol. 7, no. 8, pp. 7265–7278, 2020.
- [31] X. Zhou, G. Wang, Y. Wang, and J. Cheng, "An approximate BER analysis for ambient backscatter communication systems with tag selection," *IEEE Access*, vol. 5, pp. 22552–22558, 2017.
- [32] D. Li, W. Peng, and F. Hu, "Capacity of backscatter communication systems with tag selection," *IEEE Trans. Veh. Technol.*, vol. 68, no. 10, pp. 10311–10314, 2019.
- [33] Y. Zhang, B. Li, F. Gao, and Z. Han, "A robust design for ultra reliable ambient backscatter communication systems," *IEEE Internet Things J.*, vol. 6, no. 5, pp. 8989–8999, 2019.
- [34] D. T. Hoang, D. Niyato, P. Wang, D. I. Kim, and Z. Han, "Ambient backscatter: A new approach to improve network performance for RF-powered cognitive radio networks," *IEEE Trans. Commun.*, vol. 65, no. 9, pp. 3659–3674, 2017.
- [35] R. Kishore, S. Gurugopinath, P. C. Sofotasios, S. Muhaidat, and N. Al-Dhahir, "Opportunistic ambient backscatter communication in RF-powered cognitive radio networks," *IEEE Trans. on Cogn. Commun. Netw.*, vol. 5, no. 2, pp. 413–426, 2019.
- [36] Y. Tao, B. Li, C. Zhao, and Y. Liang, "Hardware-efficient signal detection for ambient backscattering communications," *IEEE Commun. Lett.*, vol. 23, no. 12, pp. 2196–2199, 2019.
- [37] A. N. Parks, A. Liu, S. Gollakota, and J. R. Smith, "Turbocharging ambient backscatter communication," *ACM SIGCOMM Computer Communication Review*, vol. 44, no. 4, pp. 619–630, 2014.
- [38] S. Ma, G. Wang, Y. Wang, and Z. Zhao, "Signal ratio detection and approximate performance analysis for ambient backscatter communication systems with multiple receiving antennas," *Mobile Networks and Applications*, vol. 23, no. 6, pp. 1478–1486, 2018.
- [39] Q. Tao, C. Zhong, X. Chen, H. Lin, and Z. Zhang, "Maximum-eigenvalue detector for multiple antenna ambient backscatter communication systems," *IEEE Trans. Veh. Technol.*, vol. 68, no. 12, pp. 12411–12415, 2019.
- [40] H. Guo, Q. Zhang, S. Xiao, and Y. Liang, "Exploiting multiple antennas for cognitive ambient backscatter communication," *IEEE Internet Things J.*, vol. 6, no. 1, pp. 765–775, 2019.
- [41] Q. Zhang, H. Guo, Y. Liang, and X. Yuan, "Constellation learning-based signal detection for ambient backscatter communication systems," *IEEE J. Sel. Areas Commun.*, vol. 37, no. 2, pp. 452–463, 2019.
- [42] Y. Q. Hu, H. Chen, S. L. Ji, and W. Q. Wang, "Ambient backscatter communication with frequency diverse array for enhanced channel capacity and detection performance," *IEEE Sensors J.*, vol. 20, no. 18, pp. 10876–10885, 2020.
- [43] G. Yang, Q. Zhang, and Y. Liang, "Cooperative ambient backscatter communications for green internet-of-things," *IEEE Internet Things J.*, vol. 5, no. 2, pp. 1116–1130, 2018.
- [44] D. Li and Y. Liang, "Adaptive ambient backscatter communication systems with MRC," *IEEE Trans. Veh. Technol.*, vol. 67, no. 12, pp. 12352–12357, 2018.
- [45] G. Yang, Y. Liang, R. Zhang, and Y. Pei, "Modulation in the air: Backscatter communication over ambient OFDM carrier," *IEEE Trans. Commun.*, vol. 66, no. 3, pp. 1219–1233, 2018.
- [46] R. Duan, R. Jantti, M. ElMossallamy, Z. Han, and M. Pan, "Multi-antenna receiver for ambient backscatter communication systems," in *2018 IEEE 19th International Workshop on Signal Processing Advances in Wireless Communications (SPAWC)*, 2018, pp. 1–5.
- [47] M. A. ElMossallamy, M. Pan, R. Jantti, K. G. Seddik, G. Y. Li, and Z. Han, "Noncoherent backscatter communications over ambient OFDM signals," *IEEE Trans. Commun.*, vol. 67, no. 5, pp. 3597–3611, 2019.
- [48] S. Shen, C. Y. Chiu, and R. D. Murch, "Multiport pixel rectenna for ambient RF energy harvesting," *IEEE Trans. Antennas Propag.*, vol. 66, no. 2, pp. 644–656, Feb. 2018.
- [49] C. Kang, W. Lee, Y. You, and H. Song, "Signal detection scheme in ambient backscatter system with multiple antennas," *IEEE Access*, vol. 5, pp. 14543–14547, 2017.
- [50] C. Chen, G. Wang, H. Guan, Y. Liang, and C. Tellambura, "Transceiver design and signal detection in backscatter communication systems with multiple-antenna tags," *IEEE Trans. Wireless Commun.*, vol. 19, no. 5, pp. 3273–3288, 2020.
- [51] C. Chen, G. Wang, P. D. Diamantoulakis, R. He, G. K. Karagiannidis, and C. Tellambura, "Signal detection and optimal antenna selection for ambient backscatter communications with multi-antenna tags," *IEEE Trans. Commun.*, vol. 68, no. 1, pp. 466–479, 2020.
- [52] A. Papoulis and S. U. Pillai, *Probability, Random Variables and Stochastic Processes*, 4th ed., New York, NY, USA: McGraw-Hill, 2002.
- [53] J. Qian, F. Gao, G. Wang, S. Jin, and H. Zhu, "Semi-coherent detection and performance analysis for ambient backscatter system," *IEEE Trans. Commun.*, vol. 65, no. 12, pp. 5266–5279, 2017.
- [54] V. Tarokh, H. Jafarkhani, and A. R. Calderbank, "Space-time block codes from orthogonal designs," *IEEE Trans. Inf. Theory*, vol. 45, no. 5, pp. 1456–1467, 1999.
- [55] S. M. Alamouti, "A simple transmit diversity technique for wireless communications," *IEEE J. Sel. Areas Commun.*, vol. 16, no. 8, pp. 1451–1458, 1998.
- [56] A. Goldsmith, *Wireless communications*, Cambridge university press, 2005.
- [57] S. Ma, G. Wang, R. Fan, and C. Tellambura, "Blind channel estimation for ambient backscatter communication systems," *IEEE Commun. Lett.*, vol. 22, no. 6, pp. 1296–1299, 2018.
- [58] S. Ma, Y. Zhu, G. Wang, and R. He, "Machine learning aided channel estimation for ambient backscatter communication systems," in *2018 IEEE International Conference on Communication Systems (ICCS)*, 2018, pp. 67–71.
- [59] T. Y. Kim and D. I. Kim, "Novel sparse-coded ambient backscatter communication for massive IoT connectivity," *Energies*, vol. 11, no. 1780, pp. 1–25, Jul. 2018.
- [60] W. Zhao, G. Wang, S. Atapattu, R. He, and Y. Liang, "Channel estimation for ambient backscatter communication systems with massive-antenna reader," *IEEE Trans. Veh. Technol.*, vol. 68, no. 8, pp. 8254–8258, 2019.
- [61] D. Mishra and E. G. Larsson, "Multi-tag backscattering to MIMO reader: Channel estimation and throughput fairness," *IEEE Trans. Wireless Commun.*, vol. 18, no. 12, pp. 5584–5599, 2019.
- [62] D. Darsena, G. Gelli, and F. Verde, "Joint channel estimation, interference cancellation, and data detection for ambient backscatter communications," in *2018 IEEE 19th International Workshop on Signal Processing Advances in Wireless Communications (SPAWC)*, 2018, pp. 1–5.
- [63] V. Tarokh and H. Jafarkhani, "A differential detection scheme for transmit diversity," *IEEE Journal on Selected Areas in Communications*, vol. 18, no. 7, pp. 1169–1174, 2000.
- [64] H. Jafarkhani and V. Tarokh, "Multiple transmit antenna differential detection from generalized orthogonal designs," *IEEE Trans. Inf. Theory*, vol. 47, no. 6, pp. 2626–2631, 2001.
- [65] S. Shen, C. Chiu, and R. D. Murch, "A dual-port triple-band L-probe microstrip patch rectenna for ambient RF energy harvesting," *IEEE Antennas Wireless Propag. Lett.*, vol. 16, pp. 3071–3074, 2017.
- [66] S. Shen and R. D. Murch, "Designing dual-port pixel antenna for ambient RF energy harvesting using genetic algorithm," in *2015 IEEE International Symposium on Antennas and Propagation USNC/URSI National Radio Science Meeting*, 2015, pp. 1286–1287.
- [67] S. Shen et al., "An ambient RF energy harvesting system where the number of antenna ports is dependent on frequency," *IEEE Trans. Microw. Theory Tech.*, vol. 67, no. 9, pp. 3821–3832, Sep. 2019.
- [68] S. Shen, Y. Zhang, C. Chiu, and R. Murch, "A triple-band high-gain multibeam ambient RF energy harvesting system utilizing hybrid combining," *IEEE Trans. Ind. Electron.*, vol. 67, no. 11, pp. 9215–9226, 2020.